Journal of Chemical Technology and Metallurgy, 58, 2, 2023, 385-393

SOLID-STATE SYNTHESIS OF HYDROXYAPATITE FROM BLACK SEA RAPANA VENOSA SHELLS

Albena Yoleva, Irena Mihailova, Stoyan Djambazov

University of Chemical Technology and Metallurgy
8 Kliment Ohridski blvd., 1756, Sofia, Bulgaria
E-mail: djam@uctm.edu

Received 18 October 2022
Accepted 20 December 2022

ABSTRACT

Hydroxyapatite (HA) is a major non-organic component of bones and is widely used as orthopaedic and dental material. It is widely used in biological materials due to the apatite-like structure of enamel, dentin, and bones. Black Sea Rapana venosa shells may be used as natural raw material for solid-state synthesis of hydroxyapatite. Huge amounts of rapana shells fall on the shores of the Black Sea and lead to environmental pollution. The wide availability and low cost of rapana shells, as well as the fact that they contain mainly calcium carbonate, make them a low-cost raw material for the solid-state synthesis of hydroxyapatite. In this paper a solid-state synthesis of hydroxyapatite from the Black Sea Rapana venosa shells and monocalcium phosphate monohydrate $Ca(H_2PO_4)_2.H_2O$ *is discussed. The raw materials previously were calcined at high temperature of 1000°C to increase their reactivity and formation of a good crystal structure. Then they were homogenized at a 1 to 1 weight ratio in ball mill. Samples with dimensions of 3 x 0.5 cm were pressed at a pressure of 50 MPa on a hydraulic press and then fired at 1180°C with 2 hours hold at maximum temperature. Synthesized hydroxyapatite was confirmed by XRD and FTIR spectroscopy analyses.*

Keywords: Rapana venosa shells, monocalcium phosphate monohydrate, solid-state synthesis, hydroxyapatite.

INTRODUCTION

Marine shellfish farming is an essential component of the global aquaculture industry with a trend for continued future growth. This industry generates significant waste products mainly in the form of shell material, which is currently underutilized and is a major source of environmental pollution. The material of the sea rapana venosa shells attracts attention due to the high content of calcium carbonate, low price, and availability provided by the rapidly growing seafood industry. Black Sea rapana venosa shells are functional biomaterials and $CaCO_3$ in them can be converted into a biogenic CaO. The most widely discussed biomedical use for them is in bone and tissue reconstruction [1 - 8]. The CaO powder from sea rapana venosa shells has been shown to have osteogenic properties and to act as a substrate on which new osteoblasts can grow and release bone [8]. Researchers have suggested that from sea shells may be formed hydroxyapatite [$Ca_{10}(PO_4)_6(OH)_2$), HA] and tricalcium phosphate [$Ca_3(PO_4)_2$, ß-TCP] which are a class of ceramic materials that are widely used in tissue regeneration and biomedical applications owing to their excellent bioactivity and biocompatibility [9 - 12]. Hydroxyapatite is a material that is classified as bioactive and used in orthopedic, dental, and maxillofacial applications. It is widely used in biological materials due to the apatite-like structure of enamel, dentin and bones. Hydroxyapatite may be applied in forms such as powders, porous blocks, and dense ceramics [13 - 17]. Hydroxyapatite can be obtained from natural marine sources such as snail shells, rapana venosa shells, anadara granosa shells, corals and others by solid state synthesis and hydrothermal synthesis [18 - 20].

The purpose of this paper is a solid-state synthesis of hydroxyapatite from Black Sea rapana venosa shells and monocalcium phosphate monohydrate $Ca(H_2PO_4)_2.H_2O$.

EXPERIMENTAL

Black Sea Rapana venosa shells are one natural raw material for solid-state synthesis of hydroxyapatite. In previous research, we have proven that rapana venosa shells contain over 98 % calcium carbonate. For the synthesis of hydroxyapatite, we first crushed and ball-milled the rapana venosa shells to a powder with particle size under 63 μm. In our previous research, we found that shell powder is decarbonized to CaO at 1000°C, so we calcined this powder at 1000°C for 1 hour to produce CaO. The other raw material for the synthesis of hydroxyapatite is monocalcium phosphate monohydrate $Ca(H_2PO_4)_2.H_2O$. It is also calcined to 1000°C and passed through a sieve with a particle size of fewer than 63 μm. Calcination at the high temperature of the starting raw materials leads to an increase in their reactivity and to the formation of a good crystal structure. Then, in a ball mill, the two powders in a weight ratio of 1:1 were homogenized and tablets with dimensions of 3 x 0.5 cm were pressed at a pressure of 50 MPa on a hydraulic press. The pressed samples were fired at 1180°C with a hold of 2 hours at the maximum temperature. Then the samples were ground to powder. For the production of dense samples from the synthesized hydroxyapatite powder and sintering additive of 5 mass % Li_2CO_3 were pressed tablets with dimensions of 3 x 0.5 cm at a pressure of 50 MPa on a hydraulic press and fired at 1100ºC for 1 hour hold at maximum temperature. To analyze the raw materials and the fired samples were used X-ray diffraction (DRON 3M diffractometer, Cu Ka radiation, wavelength 1.7903 Å, 28 mA current and 40 kV voltage) and FTIR spectroscopy (apparatus "Perkin-Elmer Spectrum1000" in the area 4000 cm^{-1} - 400 cm^{-1}). The microstructures of the synthesis hydroxyapatite powder and the sintered hydroxyapatite samples were studied by a scanning electron microscope Tescan FIB-SEM LYRA operated at 20 kV acceleration voltage.

RESULTS AND DISCUSSION

Fig. 1 and Fig. 2 illustrate XRD of the initial raw materials. In Fig. 1 XRD of rapana venosa shells is observed that the predominant crystalline phase ≈ 82 % is calcite ($CaCO_3$, PDF # 05-0586). The other phase that is detected is aragonite ($CaCO_3$, PDF # 41-1475). XRD of monocalcium phosphate monohydrate is shown in Fig. 2. On the diffractogram, only peaks characteristic for monocalcium phosphate monohydrate ($Ca(H_2PO_4)_2.H_2O$, PDF # 09-0347) are observed.

Figs. 3 and 4 show diffractograms of the initial calcined raw materials. After calcination at 1000°C the shells contain over 95 % calcium oxide (CaO, PDF # 37-1497) and 5 % portlandite (CaOH, PDF # 01-070-5492). On the diffractogram of the calcined at 1000°C monocalcium phosphate monohydrate, delta (d-$Ca(PO_3)_2$, PDF # 09-0363) and alpha a-($Ca(PO_3)_2$) metacalcium phosphate were detected [21]. There is

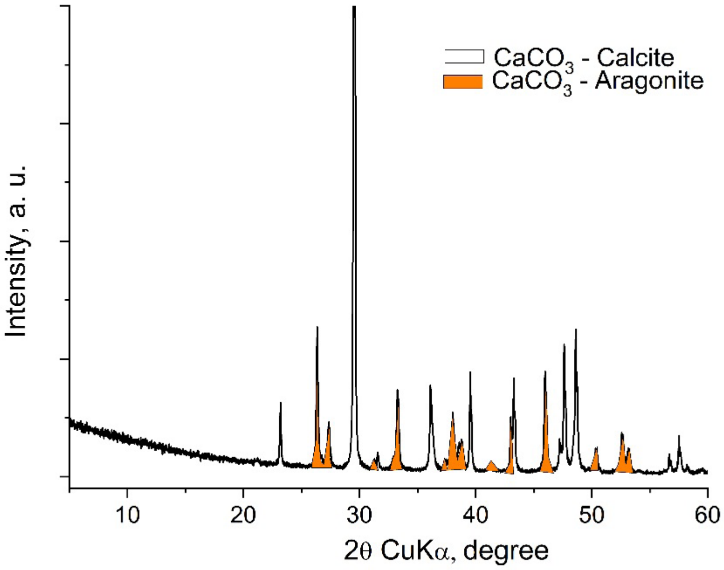

Fig. 1. Powder X-ray diffractogram of rapana shells.

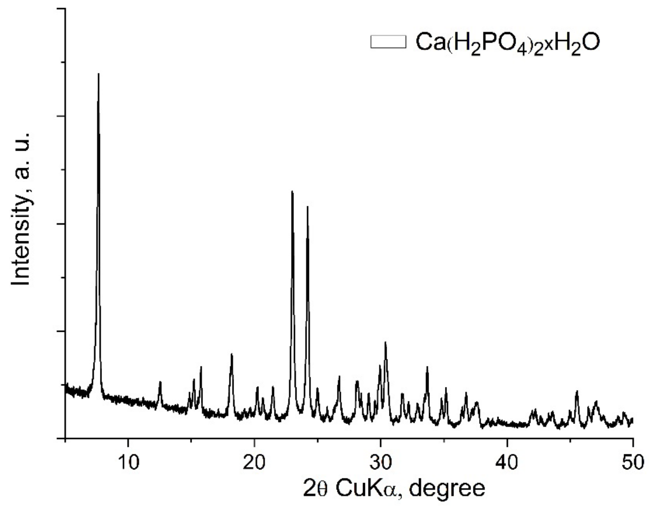

Fig. 2. Powder X-ray diffractogram of monocalcium phosphate monohydrate.

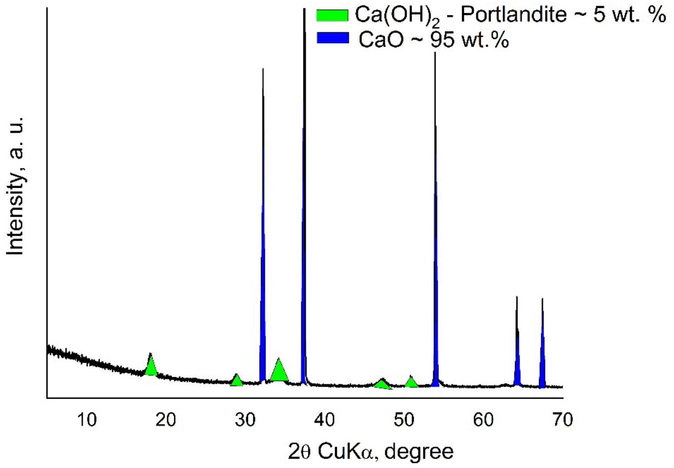

Fig. 3. Powder X-ray diffractogram of powdered rapana shells calcined at 1000°C, 1 hour.

no dispute in the literature regarding the conversion of monocalcium phosphate monohydrate to calcium metaphosphates as a result of heat treatment. On the other hand, the question of polymorphic transformations of metaphosphates is complex and unclear. The position of the most intense peaks of the diffractogram in Fig. 4 do not match to those of the phases a-$Ca(PO_3)_2$ and b-$Ca(PO_3)_2$, which are expected at the corresponding heating temperature.

Figs. 5 and 6 show the FTIR spectra of the calcined raw materials. The FTIR spectrum of powdered rapana shells calcined at 1000°C for 1 hour is shown in Fig. 5. The narrow absorption band at 3641 cm^{-1} is due to stretching mode of O-H in the structure of portlandite $Ca(OH)_2$ [22]. The absorption bands at 1480-1420 cm^{-1} and at 870 cm^{-1} are assigned to vibration modes C-O of carbonate groups CO_3^{2-} [22, 23]. This is indication for slight carbonation of the sample in the air. Moreover, there are some bands in the spectra at 1648 cm^{-1} and ≈ 3412 cm^{-1} which could be attributed to HOH deformation and to O-H stretching vibrations of water molecules.

The FTIR spectrum of monocalcium phosphate monohydrate after calcination shows also three set of bands, ranging from 471 cm^{-1} to 800 cm^{-1}, 940 cm^{-1}

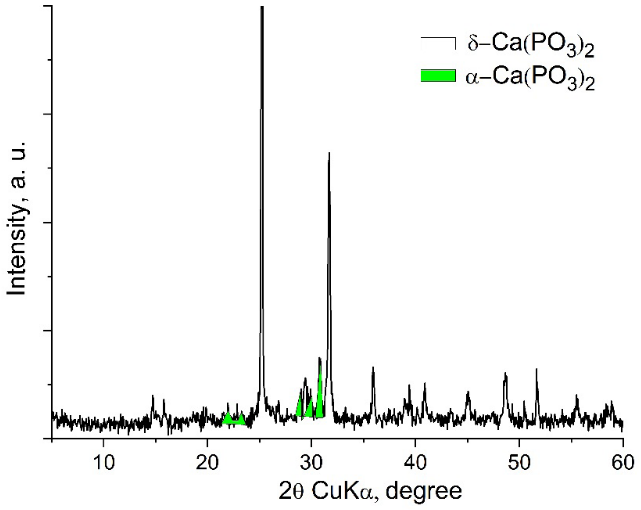

Fig. 4. Powder X-ray diffractogram of mono calcium phosphate monohydrate calcined at 1000°C, 1 hour.

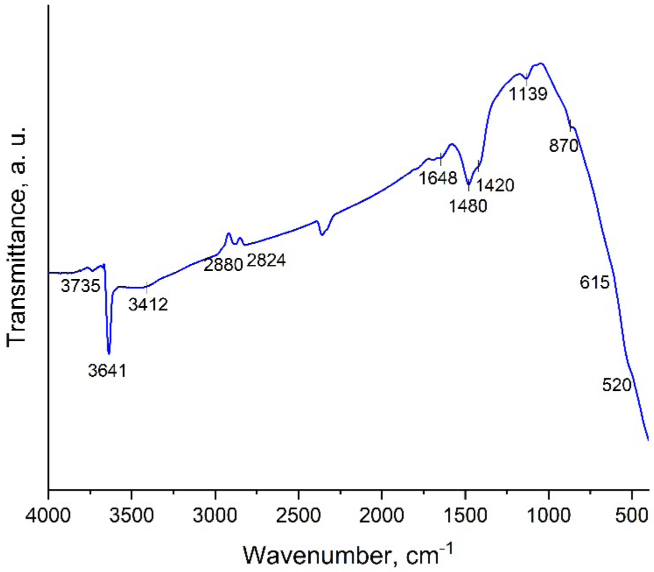

Fig. 5. FTIR spectrum of powdered rapana shells calcined at 1000°C, 1 hour.

to1084 cm^{-1} and 1114 cm^{-1} to 1629 cm^{-1}, in accordance with Moustafa el al. [24]. The bands posited at 471 cm^{-1}, 491 cm^{-1}, 551 cm^{-1} and 567 cm^{-1} can be ascribed to the bending vibration or bending phosphorus such as O-P-O and O=P-O [24]. The band at 534 cm^{-1} could be detected as O=P-O bending mode [24] and those at 713 cm^{-1} , 755 cm^{-1} and 800 cm^{-1} can be related to the symmetric stretch of O-P-O bridges (ν P-O-P) in compliance with [24]. The band at 940 cm^{-1} and a band with very small intensity at 1002 cm^{-1} can be ascribed to PO$_3$ stretching vibrations [24 - 27]. The bands at 1034 cm^{-1}, 1084 cm^{-1}, 1114 cm^{-1} could be related to the ν_{as} P-O-P [24] and symmetric stretching PO$_2$ [24, 25]. The band with very small intensity, centered at 1247 cm^{-1} can be correlated to the bridging PO$_2$ antisymmetric stretching vibration [25]. On the other hand, the bands posited at 1269 cm^{-1} and 1629 cm^{-1} can be assigned to the presence of ν_{as}PO$_2$ [24, 25, 27] and P-OH [24]. In addition, the bands, centered at 471 cm^{-1}, 559 cm^{-1}, 718 cm^{-1}, 750 cm^{-1}, and 946 cm^{-1} could be rated also to the Ca(PO$_3$)$_2$ in accordance with our XRD data.

XRD of synthesized at 1180°C hydroxyapatite, presented in Fig. 7, confirmed the formation only of one crystal phase of HA (PDF # 01-089-6440). The FTIR

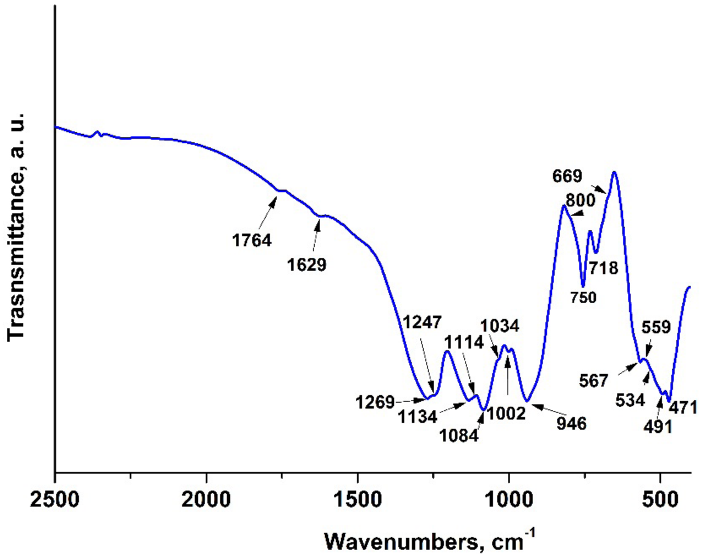

Fig. 6. FTIR spectrum of powdered monocalcium phosphate monohydrate calcined at 1000°C.

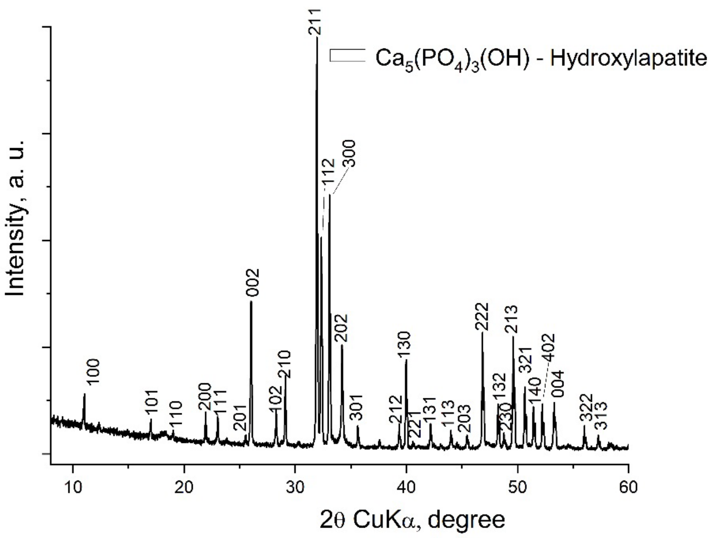

Fig. 7. Powder X-ray diffractogram of hydroxyapatite synthesized at 1180°C, 2 hour at maximum temperature.

spectrum of the synthesized hydroxyapatite is shown in Fig. 8.

There are four infrared active vibrational modes for phosphate ions n_1, n_2, n_3 and n_4 [28 - 30]. In the infrared spectrum of hydroxyapatite powder the n_3 band has two sites present at 1090 cm^{-1} and 1044 cm^{-1}. Phosphate n_1 band is present at 961 cm^{-1}. Phosphate n_4 band has three sites observed at 631 cm^{-1}, 601 cm^{-1} and 569 cm^{-1}. According to some researchers [30], the band at 631 cm^{-1} in the apatite spectrum refers to OH$^-$ oscillations. The weak band at 471 cm^{-1} is in the region of phosphate n_2 bands. The number and positions of the phosphate bands of infrared spectrum are characteristic for hydroxyapatite in accordance to [28]. The OH$^-$ band visible at 3569 cm^{-1} (O-H stretching) is also a characteristic feature of the apatite spectrum. Assignment of observed infrared band positions for synthesized hydroxylapatite powder is given in Table 1. Carbonate ions occupy two structural sites in carbonated apatite. Characteristic carbonate absorption corresponding to the CO$_3$ n_2 and CO$_3$ n_3 infrared active vibration modes can be observed respectively around 840 cm^{-1} - 900 cm^{-1} (873 cm^{-1}) and 1300 cm^{-1} - 1650 cm^{-1} [28, 29]. The shoulder detected in the spectrum at 879 cm^{-1} is assigned to the CO$_3$ n_2.

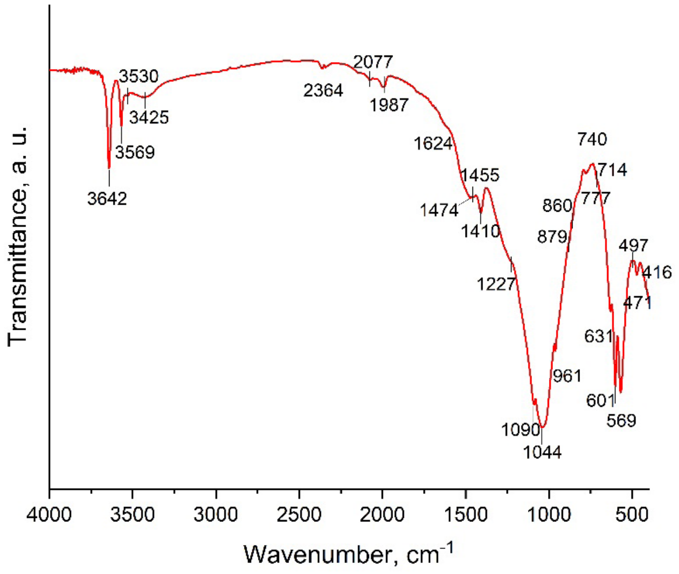

Fig. 8. FTIR spectrum of hydroxyapatite synthesized at 1180°C, 2 hour at maximum temperature.

Table 1. Observed infrared band positions for synthesized hydroxylapatite powder.

Observed band position	Peak assignment	Ref.
3642	O-H stretching characteristic for $Ca(OH)_2$	22
3569	Hydroxyl stretch	28
3530	O-H stretching vibrations of water molecules	29
3425		
1624	HOH deformation	
1455	$n_3\,CO_3^{2-}$	28
1410	$n_3\,CO_3^{2-}$	28
1090	$n_3\,PO_4^{3-}$ (asymmetric valence mode)	28, 29
1044		
961	$n_1\,PO_4^{3-}$ (symmetric valence mode)	28
879 shoulder	$n_2\,CO_3^{2-}$	30
860 shoulder	$n_2\,CO_3^{2-}$	32
777	n P-O-P linkages	31
740	symmetric valence oscillations of the P-O-P bridge bonds, formed by condensation of the PO_4^{3-} tetrahedron	33
714	n P-O-P linkages	31
631	$n_4PO_4^{3-}$ (asymmetric deformation mode)	28, 29
601		
569		
471	$n_2\,PO_4^{3-}$	28
416 shoulder	$n_2\,PO_4^{3-}$	34, 35

The occupancy of the n_2 sites depends on competition between the OH^- and CO_3^{2-} groups [28]. On the other hand, it is possible that the shoulder at 879 cm^{-1} may be due to P-OH stretching vibration of HPO_4^{2-} [30]. The occupancy of n_3 is considered to occur competitively between PO_4^{3-} and CO_3^{2-}. The observed bands in the region 1400 cm^{-1} - 1500 cm^{-1} are assigned to CO_3 n_2 as well as to surface carbonate ions. In addition to bands that refer to structural groups in the composition of the apatite phase, bands that refer to other phases are found in the experimental infrared spectrum. The well-defined band at 3642 cm^{-1} is related to the O-H stretching mode in the structure of $Ca(OH)_2$. Water bands are also seen ~ 3425 cm^{-1}.

SEM pictures of synthesized at 1180°C hydroxyapatite and sintered with 5 mass % Li_2CO_3 additive are shown in Figs. 9 and 10, respectively. The SEM image, presented in Fig 9, shows a homogeneous porous structure with a grain size below 10 microns. Idiomorphic crystals of various sizes are observed, with a predominance of those 4 - 5 microns in size. In Fig. 10 a sintered dense hydroxyapatite ceramic is visible.

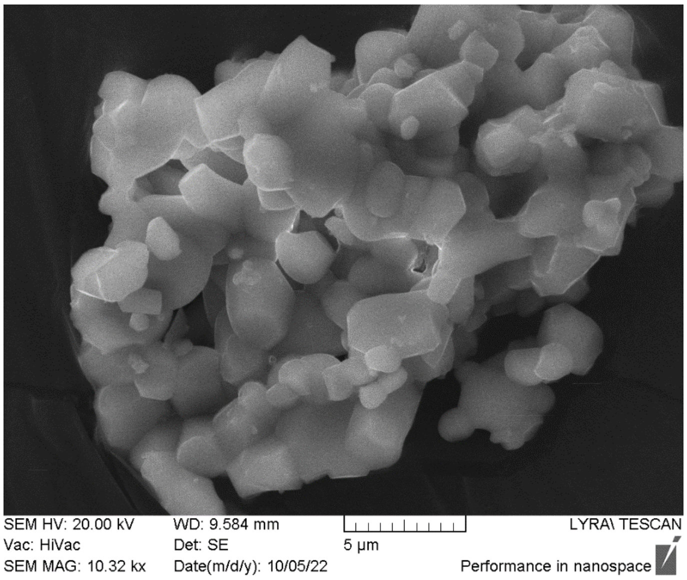

Fig. 9. SEM of synthesized at 1180°C hydroxyapatite powder.

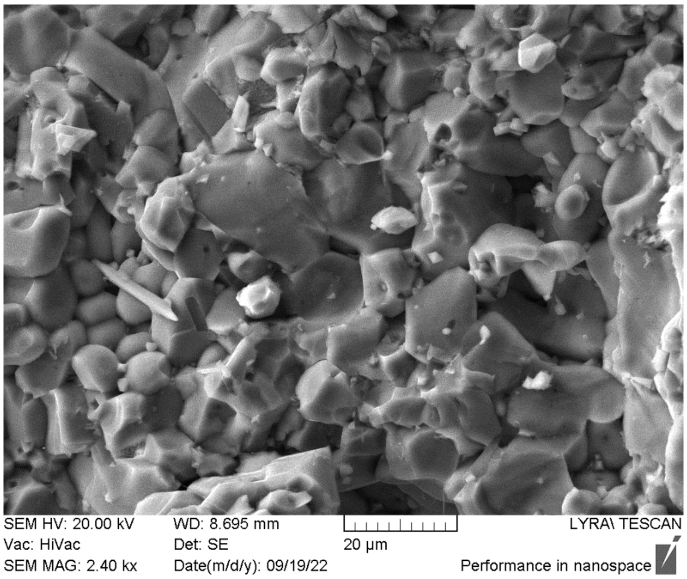

Fig. 10. SEM of sintered at 1100°C hydroxyapatite ceramic.

CONCLUSIONS

With the present experiment, we proved that the Black Sea rapana venosa shells could be used as initial material for the solid-phase synthesis of hydroxyapatite. Hydroxyapatite was successfully obtained by solid-state synthesis from rapana shells and monocalcium phosphate monohydrate after firing at 1180°C with a hold of 2 hours at the maximum temperature. The synthesized hydroxyapatite was proven using the XRD, FTIR spectroscopy, and SEM methods. A hydroxyapatite ceramic was also obtained after sintering the hydroxyapatite powder with addition of lithium carbonate at 1100°C heating for 1 hour at the maximum temperature.

REFERENCES

1. M.S. Clark, L.S. Peck, J. Arivalagan, T. Backeljau, S. Berland, J.C.R. Cardoso, C. Caurcel, G. Chapelle, M. De Noia, S. Dupont, K. Gharbi, J.I. Hoffman, K.S. Last, A. Marie, F. Melzner, K. Michalek, J. Morris, D.M. Power, K. Ramesh, T. Sanders, K. Sillanpää, V.A. Sleight, P.J. Stewart-Sinclair, K. Sundell, L. Telesca, D.L.J. Vendrami, A.Ventura, T.A. Wilding, T. Yarra, E.M. Harper, Deciphering mollusc shell production: the roles of genetic mechanisms through to ecology, aquaculture and biomimetics, Biological Reviews, 95, 2020, 1812-1837.
2. G. Magnabosco, D. Giuri, A. Bisceglie, F. Scarpino, S. Fermani, C. Tomasini, G. Falini, New Material Perspective for Waste Seashells by Covalent Functionalization, ACS Sustainable Chem. Eng., 9, 2021, 6203-6208.
3. L. Habte, M. Khan, N. Shiferaw, A. Faroo, M. Lee, S. Jung, J. Ahn, Synthesis, Characterization and Mechanism Study of Green Aragonite Crystals from Waste Biomaterials as Calcium Supplement, Sustainability, 12, 2020, 5062-5072.
4. M. Ravi, B. Murugesan, A. Jeyakumar, K. Raparthi, A review on utilizing the marine biorefinery waste in construction raw materials to reduce land pollution and enhance green environment, Advances in Materials Science, 21, 3, 2021, 44-62.
5. M. Jović, M. Mandić, M. Sljivić-Ivanović, I. Smičiklas, Recent trends in application of shell waste from mariculture, Studia Marina, 32, 1, 2019, 47-62.
6. U. Anjaneyulu1, D. Pattanayak, U. Vijayalakshmi, Snail shell derived natural hydroxyapatite, Materials and Manufacturing Processes, 31, 25, 2016, 206-216.
7. J. Morris, T. Backeljau, G. Chapelle, Shells from aquaculture: a valuable biomaterial, not a nuisance waste product, Reviews in Aquaculture, 11, 2019, 42-57.
8. Z. Zuliantoni, W. Suprapto, P. Setyarini, F. Gapsari, Extraction and characterization of snail shell waste hydroxyapatite, Results in Engineering, 14, 2022, 100390.
9. E. Fiume, G. Magnaterra, A. Rahdar, E. Vernéand Francesco Baino, Hydroxyapatite for Biomedical Applications: A Short Overview, Ceramics, 4, 2021, 542-563.
10. J. Jeong, J. Kim, J. Shim, N. Hwang, C. Heo, Bioactive calcium phosphate materials and applications in boneregeneration, Biomater. Res., 23, 4, 2019, 6-11.
11. S.V. Dorozhkin, Calcium orthophosphate bioceramics, Ceram. Int., 41, 2015, 13913-13966.
12. B. Carvalho, E. Rompen, G.Lecloux, P. Schupbach, E. Dory, Effect of sintering on in vivo biological performance of bovine hydroxyapatite, Materials, 12, 2019, 3946-3960.
13. R. Owen, M. Dard, H. Larjava, Hydoxyapatite/beta-tricalcium phosphate biphasic ceramics as regenerative material for therepair of complex bone defects, J. Biomed. Mater. Res. B Appl. Biomater., 106, 2018, 2493-2512.
14. A. Szczes; L. Hołysz, E. Chibowski, Synthesis of hydroxyapatite for biomedical applications, Adv. Colloid Interface Sci., 249, 2017, 321-330.
15. F. Baino, G. Magnaterra, E. Fiume, A. Schiavi, L. Tofan, Schwentenwein, M., E. Verné, Digital light processing stereolithography of hydroxyapatite scaffolds with bone-like architecture, permeability, and mechanical properties, J. Am. Ceram. Soc. 105, 2022, 1648-1657.
16. H. Javadinejad, R. Kahrizsangi, Thermal and kinetic study of hydroxyapatite formation by solid-state reaction, Int. J. Chem. Kinetics, 53, 5, 2021, 583-595.
17. N. Mohd Pu'ad, R. Abdul, H. Mohd, H. Abdullah, M. Idris, T. Lee, Synthesis method of hydroxyapatite: A review, Materials Today, Proceedings 29, 2020, 233-239.
18. A. Shavandi, A. Bekhit, A. Sun, Synthesis of nano-hydroxyapatite (nHA) from waste mussel shells using

a rapid microwave method, Materials Chemistry and Physics, 150, 2015, 607-616.

19. B. Musa, I. Raya, H. Natsir, Synthesis and Characterizations of Hydroxyapatite Derived Blood Clam Shells (Anadara granosa) and Its Potency to Dental Remineralizations, International Journal of Applied Chemistry, 12, 4, 2016, 527-538.
20. I. Antoniac, I. Lesci, A. Blajan, G. Vitioanu, A. Antonia, Bioceramics and biocomposites from marine sources, Key Engineering Materials, 672, 2015, 276-292.
21. A. McIntosh, W. Jablonski, X-ray diffraction powder patterns of calcium phosphates, Analytical Chemistry, 28, 9, 1956, 1424-1427.
22. M. Khachani, A. El Hamidi, M. Halim, S. Arsalane, Non-isothermal kinetic and thermodynamic studies of the dehydroxylation process of synthetic calcium hydroxide $Ca(OH)_2$, J. Mater. Environ. Sci., 5, 2, 2014, 615-624.
23. T. Liu, Y. Zhu, X. Zhang, To Zhang, Ta Zhang, Synthesis and characterization of calcium hydroxide nanoparticles by hydrogen plasma-metal reaction method, Mater. Lett., 64, 23, 2010, 2575-2577.
24. Y.M. Moustafa, K. El-Egili, Infrared spectra of sodium phosphate glasses, J. Non-Cryst. Solids, 240, 1998, 144-153.
25. S. El Makhloufy, R. Oubouaza, A. Ouasri, S. Belaaouad, X-Ray Diffraction and Infrared Spectroscopy Data Review Analyses of the Calcium Phosphates, Biointerface Res. Appl. Chem., 12, 1, 2022, 732-755.
26. A. Bertoluzza, S. Cacciari, A. Tinti, M. Vasina, M. A. Morelli, FTIR and Raman spectra of bioceramics obtained by an innovative method, J Mat. Sci.: Materials in Medicine, 6, 1995, 76-79.
27. E.A. Abou Neel, W. Chrzanowski, D.M. Pickup, L.A. O'Dell, N.J. Mordan, R. J. Newport, M.E. Smith, J.C. Knowles, Structure and properties of strontium-doped phosphate-based glasses, J. R. Soc, Interface, 6, 34, 2009, 435-446.
28. I. Rehman, W. Bonfield, Characterization of hydroxyapatite and carbonated apatite by photo acoustic FTIR spectroscopy, J. Mat. Sci.: Materials in Medicine 8, 1997, 1-4.
29. M. Veiderma, R. Knubovets, K. Tonsaadu, Structural properties of apatites from Finland studied by FTIR spectroscopy, Bulletin of the Geological Society of Finland, 1998, 69-75.
30. A. Grunenwald, C. Keyser, A-M Sautereau, E. Crubézy, B. Ludes, C. Drouet, Revisiting carbonate quantification in apatite (bio)minerals: a validated FTIR methodology, J. Archaeol. Sci., 49, 2014, 134-141.
31. M.A. Cherbib, I. Khattech, L. Montagne, B. Revel, M. Jemal, M.A. Cherbib, I. Khattech, L. Montagne, B. Revel, M. Jemal, Structure properties relationship in calcium sodium metaphosphate and polyphosphate glasses, J. Non-Cryst. Solids, 485, 2018, 1-13.
32. E.P. Paschalis, E. DiCarlo, F. Betts, P. Sherman, R. Mendelsohn, A.L. Boskey, FTIR microspectroscopic analysis of human osteonal bone, Calcif. Tissue Int., 59, 1996, 480-487.
33. R. Knubovets, Structural mineralogy and properties of natural phosphates, Rev. Chem. Eng., 9, 9, 1993, 161-216.
34. F. Bollino, E. Armenia, E. Tranquillo, Zirconia/Hydroxyapatite Composites Synthesized Via Sol-Gel: Influence of Hydroxyapatite Content and Heating on Their Biological Properties, Materials, 10, 7, 2017, 757.
35. F.A. Shah, Towards refining Raman spectroscopy-based assessment of bone composition. Sci. Rep., 10, 2020, 16662.